REFINEMENT OF A DRONE-BASED METHOD FOR ESTIMATING COARSE WOODY DEBRIS AND BIOMASS RESIDUE FOLLOWING FOREST HARVEST

by

BRIAN DAVIS

(Under the Direction of Lawrence Morris)

ABSTRACT

A quick and reliable method to estimate coarse woody debris (CWD) following forest harvest is required. Current methods of estimation are both time consuming and costly. A previous study tried to develop a method to calculate CWD volume using drones but overestimated volumes significantly. This study sought to reduce the errors of the previous study. Plots and piles were measured at two recently harvested sites in Emanuel and Effingham counties in Georgia, USA. Errors in estimates of volume ranged from very good (<10%) to very poor (>70%). Analysis showed no significant difference in ground and GIS measurements for distributed slash for the Emanuel County plots ($p = 0.7362$, $df = 8$) and for the Effingham County plots ($p = 0.6467$, $df = 9$). Ground-based measurements were significantly different from GIS measurements at both Rimes and Jack's Creek for both oriented and slash piles ($p = 0.0039$, $df = 15$).

INDEX WORDS: Forest inventory, unmanned aerial system, unmanned aerial vehicle, bioenergy, forest products

REFINEMENT OF A DRONE-BASED METHOD FOR ESTIMATING COARSE WOODY DEBRIS AND BIOMASS RESIDUE FOLLOWING FOREST HARVEST

by

BRIAN DAVIS

BS, University of Georgia, Daniel B. Warnell School of Forestry and Natural Resources, 2015

A Thesis Submitted to the Graduate Faculty of The University of Georgia in Partial Fulfillment of the Requirements for the Degree

MASTER OF SCIENCE

ATHENS, GEORGIA

2017

REFINEMENT OF A DRONE-BASED METHOD FOR ESTIMATING COARSE WOODY DEBRIS AND BIOMASS RESIDUE FOLLOWING FOREST HARVEST

by

BRIAN DAVIS

Major Professor:	Lawrence Morris
Committee:	Roger Lowe III
	Marguerite Madden
	Cristian Montes

Electronic Version Approved:

Suzanne Barbour
Dean of the Graduate School
The University of Georgia
August 2017

DEDICATION

I wish to dedicate this work to my family without whose support I would have never even begun this journey. Thank you to my wife, Josie, for your continued support as I make my way in the world. Thank you to my daughter, Mary Mardell, for the love you have provided to me throughout your three years on this earth. You mean the world to me. Thank you to my parents, George and Mary Ellen, for your support, both emotional and financial, as I made the transition back to academic life.

ACKNOWLEDGEMENTS

I would like to thank Dr. Lawrence Morris and Dr. Roger Lowe III for offering me this project. I appreciate the support you have given me as we worked through the project. I would especially like to thank Dr. Lowe for helping me to gain the GIS skills necessary to complete this project. I would like to thank my other committee members, Dr. Madden and Dr. Montes, for their support and guidance. I would also like to thank Dr. Jordan and Dr. Bernardes from the Center for Geospatial Research. Dr. Jordan did extensive work on the previous project. Dr. Bernardes offered some insight on possible ways to reduce error and refine approaches.

TABLE OF CONTENTS

Page

LIST OF TABLES

Page

LIST OF FIGURES

Page

CHAPTER 1

INTRODUCTION

1.1 Background

Harvest residue plays an important role in managed forest systems. Foliage and woody debris, also known as coarse woody debris (CWD), protect physical properties of the mineral soil (e.g. porosity, infiltration rate), moderate temperature extremes, reduce surface evaporation and improve water relations. Partially because of the more moderate environmental conditions surface debris impart, it creates habitat for an assemblage of macro, meso and micro fauna [1]. It provides the carbon and energy source of the detrital food web [2]. Within mineral soil horizons, organic matter contributes to soil development through production of organic acids and stabilization of structure, through its contribution to water holding capacity, and nutrient retention and release, and as the primary soil reservoir of several plant nutrients [3]. Thus, management activities that alter the quantity and distribution of organic matter have ramifications both for forest productivity and ecosystem functions [4] as well as for global carbon cycles.

Pine forests of the southern US are a major source of woody debris residues used for bioenergy [5]. In 2012, approximately 40% of the world's biomass fuel, in the form of wood pellets created from CWD harvest, was exported from the United States to Europe [6], most from the southern US. Estimates are that 60% of the world renewable energy could be in the form of biomass fuel by 2030 [7]. With such a large and growing

market for biomass fuel, the need for accurate, quick estimation of CWD residue has never been greater. From an operational standpoint, contractors need a means of estimating biomass to plan harvests and schedule equipment. From a regulatory standpoint, estimates of retained biomass are needed to ensure compliance with biomass retention guidelines.

Current methods of field sampling woody debris residues, such as line intersect sampling (LIS) [8], are time consuming and inaccurate, especially when compared to the costs. Researchers have estimated that LIS must have transects of at least 100 meters to achieve coefficients of variation less than 100% for a 1 ha site [9]. New methods to estimate biomass residue estimation that are quicker and more accurate are required to keep up with the growing demand for biomass harvested following traditional pulp and sawtimber harvests. One method that shows promise for quickly estimating biomass residue is the use of unmanned aerial vehicles (UAVs), also known as drones. Compared with current methods, UAVs allow more area to be analyzed at relatively low cost and in less time than traditional field sampling. This project sought to develop a procedure for estimating post-harvest residues volumes from photo images collected using low cost drones that achieved as good, or better, results than traditional field sampling.

1.2 Current Methods of Volume Estimation

Woody debris residues from timber harvest are often poorly estimated, as costs dictate that more emphasis be placed on timber collection and transportation [10]. On most harvested sites, two distinct conditions must be evaluated: i) volume of residues dispersed as individual pieces scattered across the site, and ii) piled residues. Currently, the LIS method is most often used to estimate scattered biomass residue, but it only

samples a limited portion of the area [11]. The wood along each transect is gathered, measured, and the measurement is put into a formula to determine total cubic volume of wood in the area. LIS is found to be most accurate when transects are longer and target areas are large [9, 12, 13]. In LIS, all wood that falls across the transect is measured and applied to the formula of Wagner [8](*Equation 1)*:

$$T = \left(\frac{1.2337}{L}\right) \cdot \sum_{i=1}^{n} d_i^2 \qquad (Equation\ 1)$$

where:

T is the cubic volume of CWD (m^3/ha)

L is the length of the transect (m)

d_i is the diameter of the i^{th} intersected piece

n is the total number of CWD pieces [8].

However, knowing that plot-level estimates of biomass using the line-transect method are extremely variable, they are not useful for comparison with drone-based estimates of biomass.

For piled debris, a waste residue survey (WRS) is used in Canada. The total area is stratified for sampling. Two or more piles in each stratum are measured using a fixed area plot (3.99-m radius). Each stem 10 cm or larger is measured and the fraction of total plot depth at which wood was measured is estimated to estimate a plot density (PD) (m^3 wood·m^{-2} plot area) for a pile. The summed pile area in a stratum is estimated from the number of piles and their corresponding area estimate. This estimate is then multiplied by the average plot density to estimate the stratum wood volume (m^3·$stratum^{-1}$). This can be converted to a site level estimate using the area of the strata. Finally, a biomass

estimate can be generated using the volume of each species multiplied by the appropriate wood density ($kg \cdot m^{-3}$) [12]. Another method of estimating pile volumes is to apply geometric equations (EEP) for each pile. In EEP, an elliptical paraboloid at 95% pile height is used to estimate the volume of a pile. This relationship between total volume and actual wood volume is known as the packing ratio (PR). It is essential to use an appropriate PR (m^3 wood $\cdot$ m^{-3}pile volume) when calculating volume using UAVs. These values are essential to mitigate error from the conversion of imagery to GIS data to volume calculation [14]. Standard PRs for a species are used to estimate the volume of wood within each pile. Using non-specific PRs results in an overestimation of pile volume [14]. Trofymow et al. [14] conducted a study comparing WRS, EEP, LiDAR and GIS methods for estimating pile volumes. They conducted a WRS and disassembled eight piles to calculate PRs and PDs. They used LiDAR data from 2011 compared with 2008 to make LiDAR volume estimates. The 2011 LiDAR ground returns were used to create a DSM in ArcGIS. Piles were manually delineated in ArcGIS. The WRS method produced significantly lower estimates (30-50%) than any other method. EEP and LiDAR estimates gave the highest values and were approximately 20% greater than GIS methods [14].

1.3 LiDAR

Light detection and ranging (LiDAR) has been used to estimate forest volume and biomass by measuring individual tree crowns [15]. LiDAR has also been shown to be useful in identifying CWD on beaches to estimate its sand storage capacity [16]. It has also been used to create digital terrain models (DTM) to calculate the volume of landslides using data from before and after a landslide event [17]. These studies have

shown that aerial data can be used to calculate volume. A drawback to LiDAR currently is cost. A LiDAR device can cost hundreds or thousands of dollars. Moreover, most LiDAR instruments are attached to airplanes requiring a plane and a pilot. The technology is advancing and some LiDAR units are suitable for mounting on UAV. Moreover, LiDAR can be more cost effective than traditional sampling methods under the right circumstances [18].

1.4 Orthophotography (GIS)

GIS, or geographic information system, technology has been used for years in multiple disciplines, such as archeology and the field of forestry and natural resources as far back as the 1960s [19]. Decision makers can use high resolution imagery obtained from satellites and airplanes in their workflow. These images when properly referenced to the earth's surface to remove topographic displacements are called orthophotos [20]. Moreover, in dealing with soil characteristics and mapping, GIS has been used in several studies [21, 22]. It has also been used to analyze ground water resources [23]. GIS has been used to map and predict cliff changes as well [24]. While the field of GIS is advancing, these methods have been used across disciplines for years. However, orthophotos and LiDAR, being traditionally collected by fixed wing aircraft, are still costly and have significant delay time from harvest to data collection.

High-resolution imagery from a UAV can create digital surface models (DSM). To create these models from images requires a photogrammetric process called structure from motion (SfM). SfM creates these models effectively, and at low cost, by combining images that overlap to provide multiple perspectives of an object [25]. UAV offer the ability to collect nearly real-time data for a landscape at a significantly reduced price.

1.5 Challenges in Use of UAV Technology for Residue Estimation

This project focuses on using UAV technology to estimate the volume of CWD available for biomass harvest following traditional merchantable stemwood harvests of southern pine plantations. Specific challenges addressed in this project deal with developing methods to overcome the microtopography, or subtle changes in elevation or surface features, at a given site and being able to accurately delineate CWD from the ground. While the UAV provides high resolution imagery, it can still be difficult to determine small changes in microtopography at the ground layer. Those small changes can result in large discrepancies between actual and calculated volume. Similarly, differing soil and vegetation types have different spectral characteristics [21]. The spectral characteristics are important because it is one of the best ways to delineate CWD from the ground in an automated process. Many factors influence soil spectral characteristics including, but not limited to, moisture and organic matter content [26]. These factors vary across a landscape. This is a case where the high resolution of the UAV imagery can be a negative. The high-resolution imagery contains a large amount of noise (e.g. rocks, bark, small sticks) that make automated classification difficult.

Another limitation to use of UAV technology for residue estimation stems from how the imagery is processed. After harvest, CWD and brush are often piled. These piles are often referred to as slash piles and consist of limbs and tree tops as noted by Manitoba Conservation [27]. When converting images from UAVs to data in GIS programs such as ESRI ArcMap™, these features are viewed as solid objects. While this is correct for individual pieces of CWD, for slash piles, this results in an overestimation

of volume. For loblolly pine (*Pinus taeda*), Beauvais [28] found that only 7.89% of total slash pile volume was CWD volume.

While the GIS transformations accurately represent CWD as a solid object, it does misrepresent the shape of CWD. The UAV imagery displays an object with a round top and squared bottom (Figure 1).

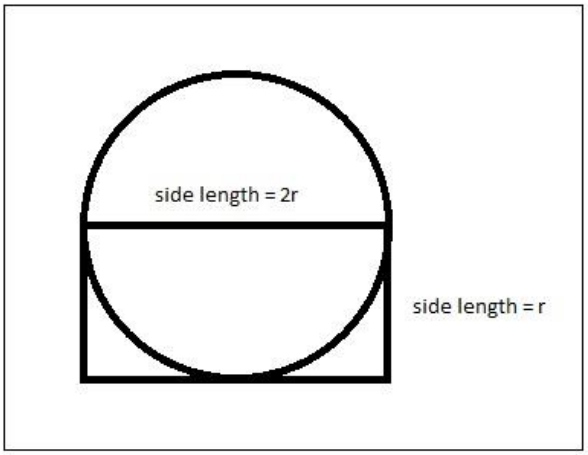

Figure 1: Example of how UAV imagery views stems and CWD. The outside boundary is what is viewed as solid while we need to calculate the area (and thus volume) of the circle alone.

Equation 2 can be used correct the calculation to eliminate the unwanted area.

where *x* is the correction factor.

$$\pi r^2 = (\pi r^2/2 + 2r \cdot r) \cdot x \qquad (Equation\ 2)$$

Through algebraic manipulation, we solve for $x = 2\pi/(\pi + 4)$, which is 0.8798. This general adjustment can be applied to all cylindrical objects viewed from UAV images, otherwise, UAV analyses will be biased to an overestimate.

CHAPTER 2

METHODS

2.1 Study Site and Plot Establishment

Field sites were located on two recently completed commercial timber harvests on lands managed by Forestry Investment Associates in Effingham and Emanuel counties, in southeast Georgia (Figure 2). The Effingham County site was called Rimes and the Emanuel County site was called Jack's Creek. These names will be used to distinguish the sites for the remainder of the paper. Both sites were in the Lower Coastal Plain on poorly to somewhat poorly drained soils and had been bedded prior to planting the recently harvested stand. Both harvested sites were approximately 11 hectares (27 acres) in size. Experience in earlier field trials suggested that plot-level estimates of biomass using the line-transect method were, themselves, too variable to be useful for comparison with drone-based estimates of biomass. Instead, on each of these two sites, ten 10 m x 10 m plots were installed within the harvested area (Figures 7 and 8). Each 10 x 10 m plot was flagged on each corner and the north corner was monumented with PVC pipe that served as the ground control points for later georeferencing. A 100% inventory of scattered residue biomass greater than or equal to 7.5 cm in diameter was completed within each of these plots. In addition to the scattered residues, oriented piles of stems

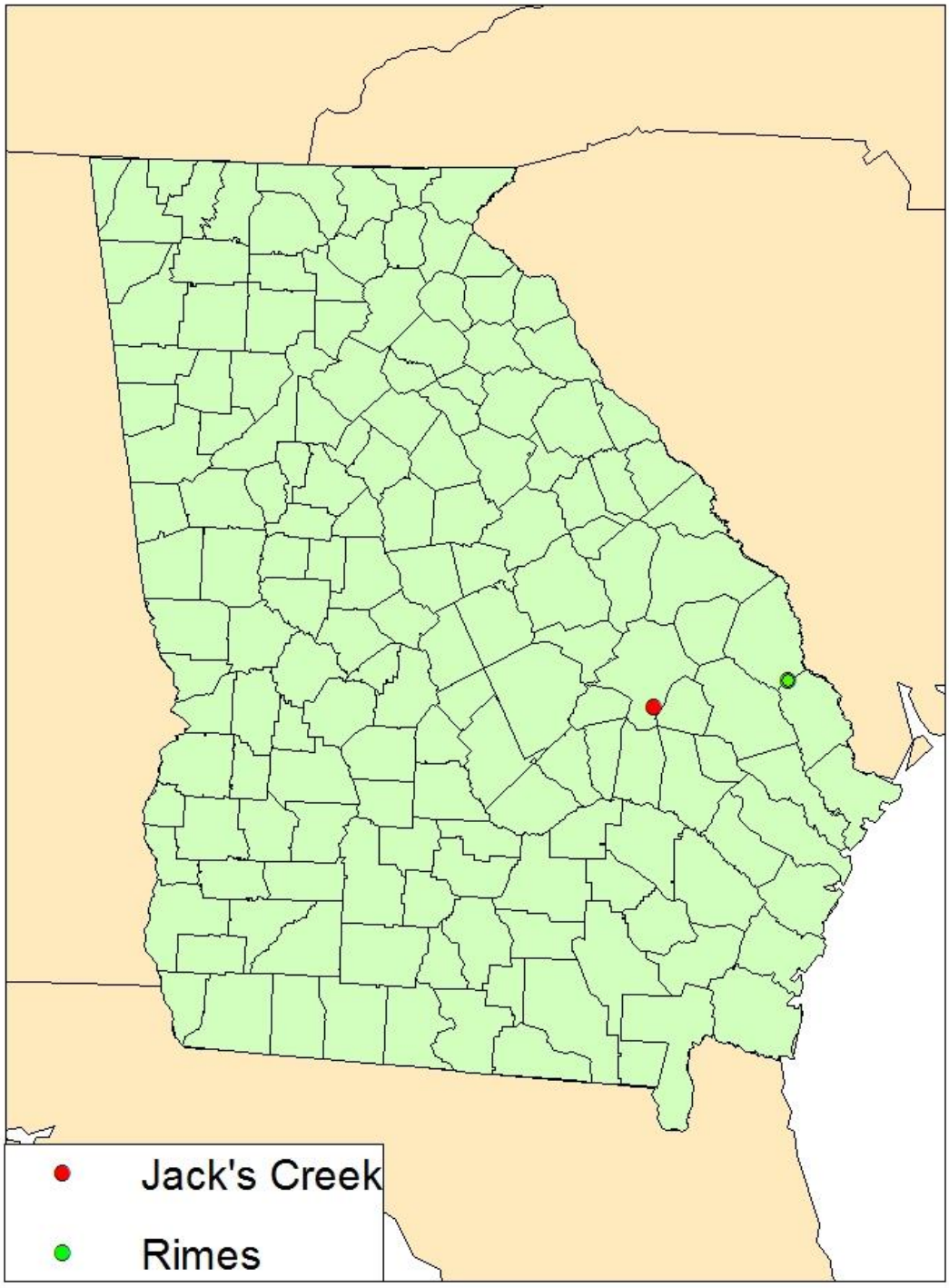

Figure 2: Map of Georgia with study sites marked.

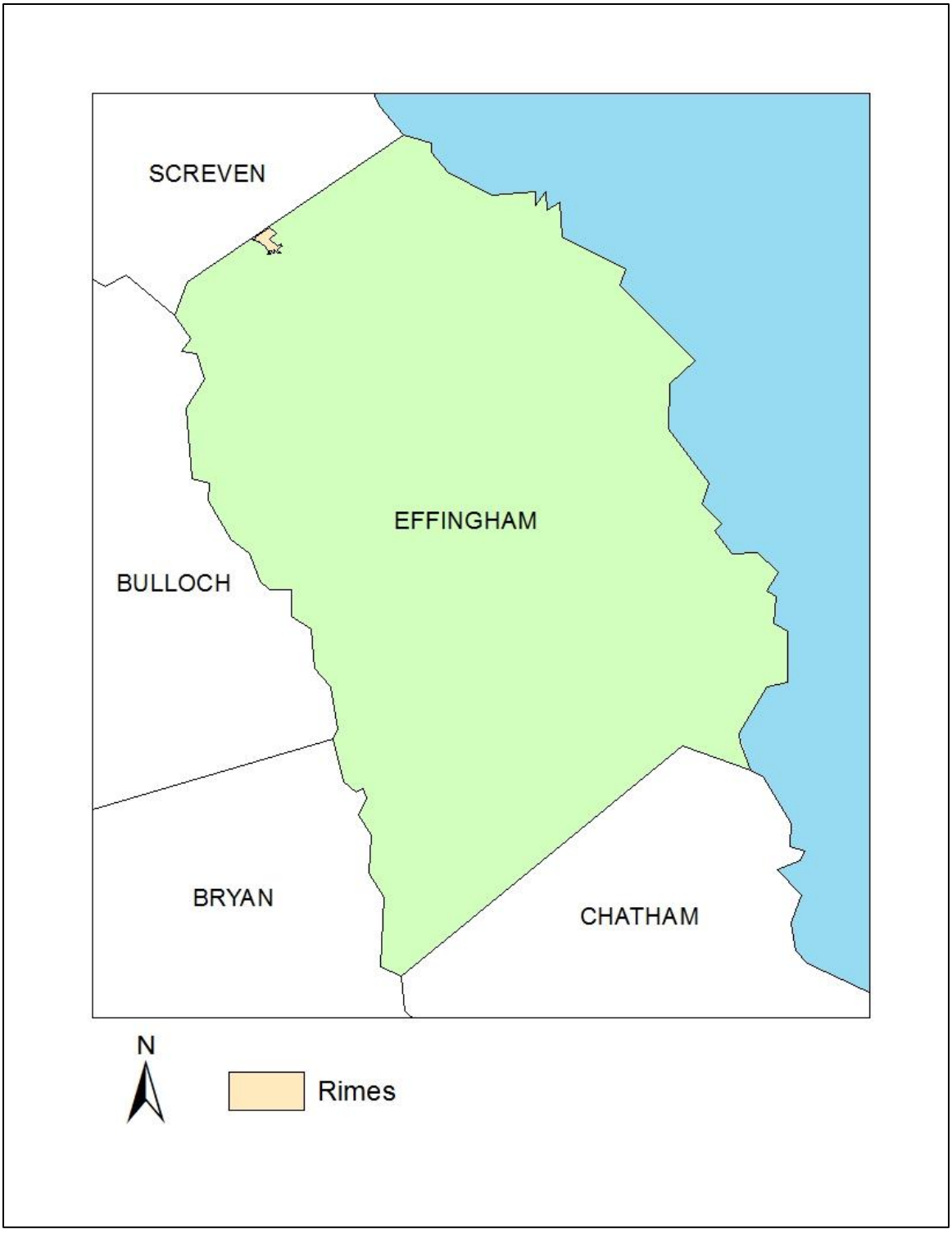

Figure 3: Rimes site within Effingham County.

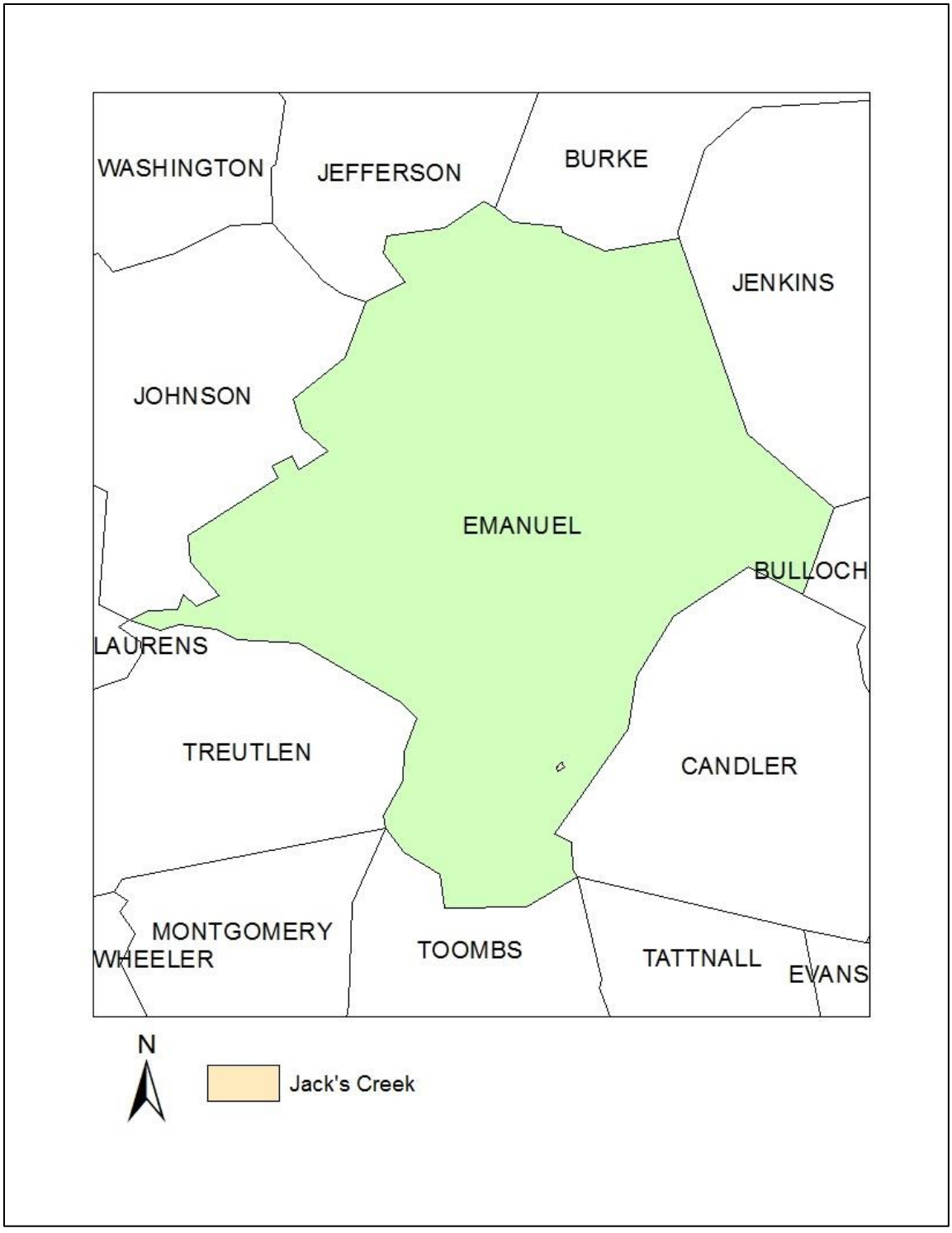

Figure 4: Jack's Creek site within Emanuel County.

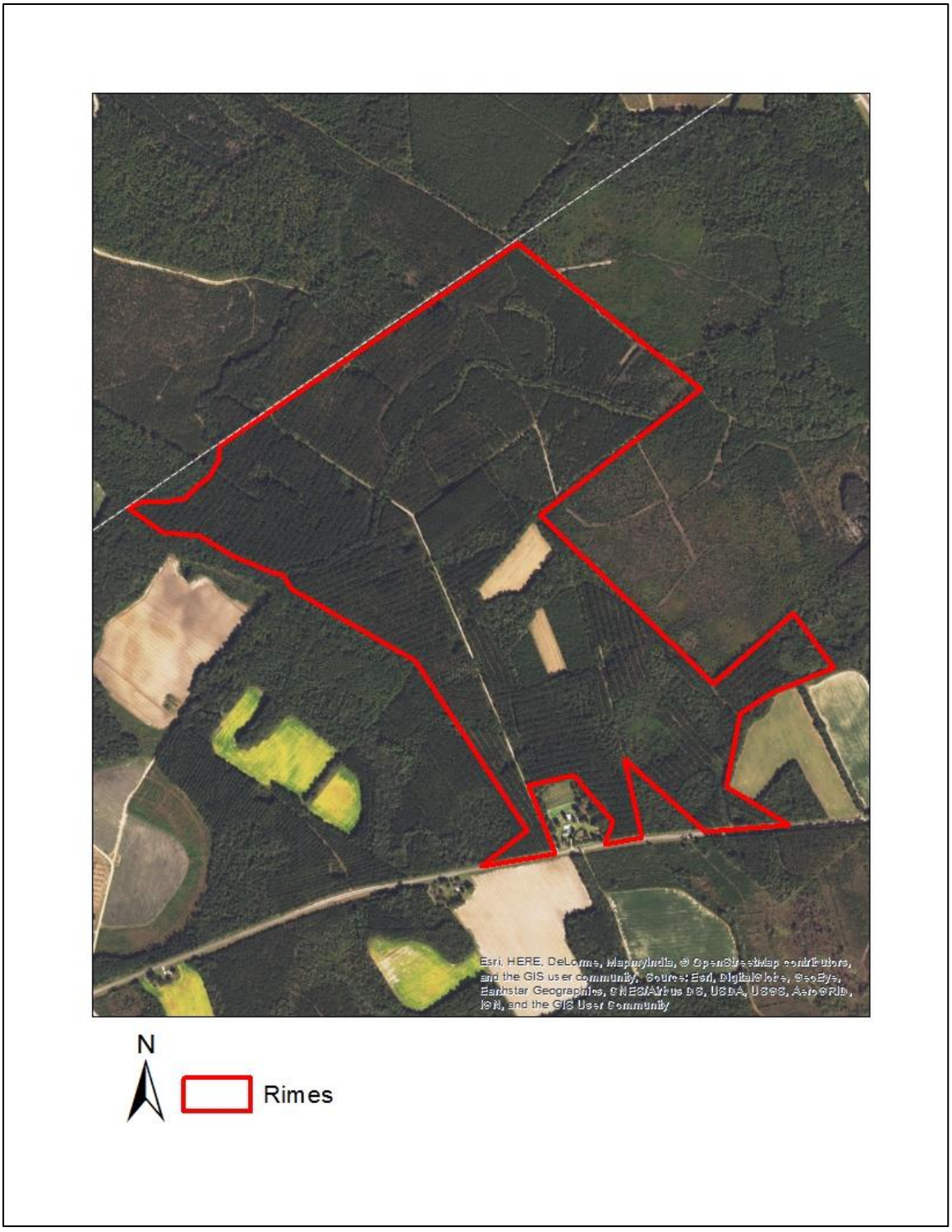

Figure 5: Rimes site with ESRI satellite imagery.

Figure 6: Jack's Creek site with ESRI satellite imagery.

occurred on the Jack's Creek site. Each stem was measured in seven of these piles. Finally, piles of slash (tops, limbs, etc.) were also measured. For these slash piles, length, width, and height were measured. Nine slash piles were measured at the Rimes site (Figures 7 and 8).

2.2 Field estimates of CWD volume

Field measurements were conducted between December 28, 2016 and January 5, 2017. Each CWD piece of 7.5 cm diameter or larger within the 10-meter x 10-meter plots was measured and the length and diameter recorded. For some plots with numerous pieces of CWD, four workers measured the CWD. For most plots, a two-person team completed measurements in 20-30 minutes. Each plot was measured at least twice, with some plots measured three times. The same two-person crew never re-measured the same plot.

In addition to the plots, oriented piles and slash piles were measured. For the oriented piles, each stem's large and small diameter was measured along with the stem length. For oriented pile volume, the frustum, the portion of a cone when the tip is removed by a plane parallel to the base, volume equation was used and individual stem volumes were summed to estimate total pile volume. For the slash piles, the total length, width, and height of the pile was measured. All piles were assumed to be half ellipsoids. The half ellipsoid volume equation of Hardy [29] was used (*Equation 3*):

$$V = \frac{\pi \cdot l \cdot w \cdot h}{6} \qquad (Equation\ 3)$$

where

V is the gross volume of the pile

l is the length of the pile

w is the width of the pile

and h is the height of the pile.

The volume was multiplied by 0.0789, which is the packing ratio from Beauvais (2010).

2.3 Data Collection

GPS coordinates for the monumented corners of each 10 x 10 m plot and all piles were measured with a high-precision Garmin GPS 17x HVS™ unit with Nomad™ data collector and the SOLO Forest™ field software prior to each flight. At each point, a minimum of 30 observations were made and coordinates were differentially corrected using Trimble Pathfinder Office and the CORS network of GPS base stations. UAV flights were conducted on January 19, 2017. Plots were flown using DJI Phantom 3 Professional™ and DJI Phantom 4™ quadcopters at 25 to 30 meters height along a standard flight path to collect the video of each plot (Figure 10). Flight paths were entered and controlled using Map Pilot™ software for IOS. Eight hundred ninety-six images were collected on the Rimes site and 1084 images were collected on the Jack's Creek site. The resolution of each image was 3000 x 4000 pixels. It took less than 1 hour from arrival to departure to complete the flights on each site. All flights were completed between 9:00 and 4:30 pm to minimize shadows caused by low sun angle.

Sidelap and endlap need to be high (minimum 70%/70%) in UAV data collection to ensure proper image coverage [30]. For this project, sidelap and endlap were set to 80% each. DSMs and orthophotos were generated for each site separately using the Agisoft PhotoScan Professional™ software, version 1.2.4 on a dual Xeon E5-2690™ workstation with 96 GB RAM.

Figure 7: Rimes plots and piles with ESRI base map.

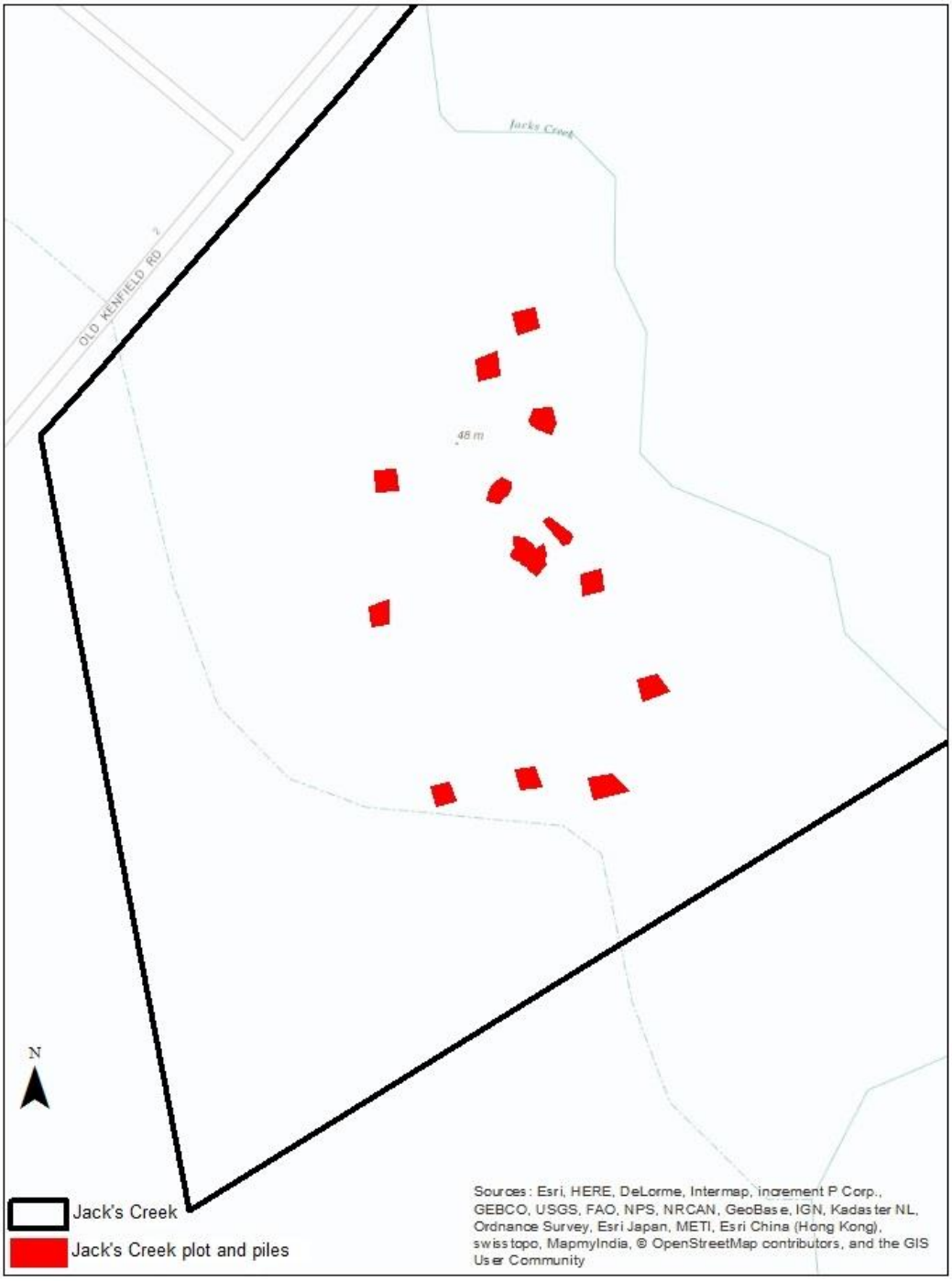

Figure 8: Jack's Creek plot and piles with ESRI base map.

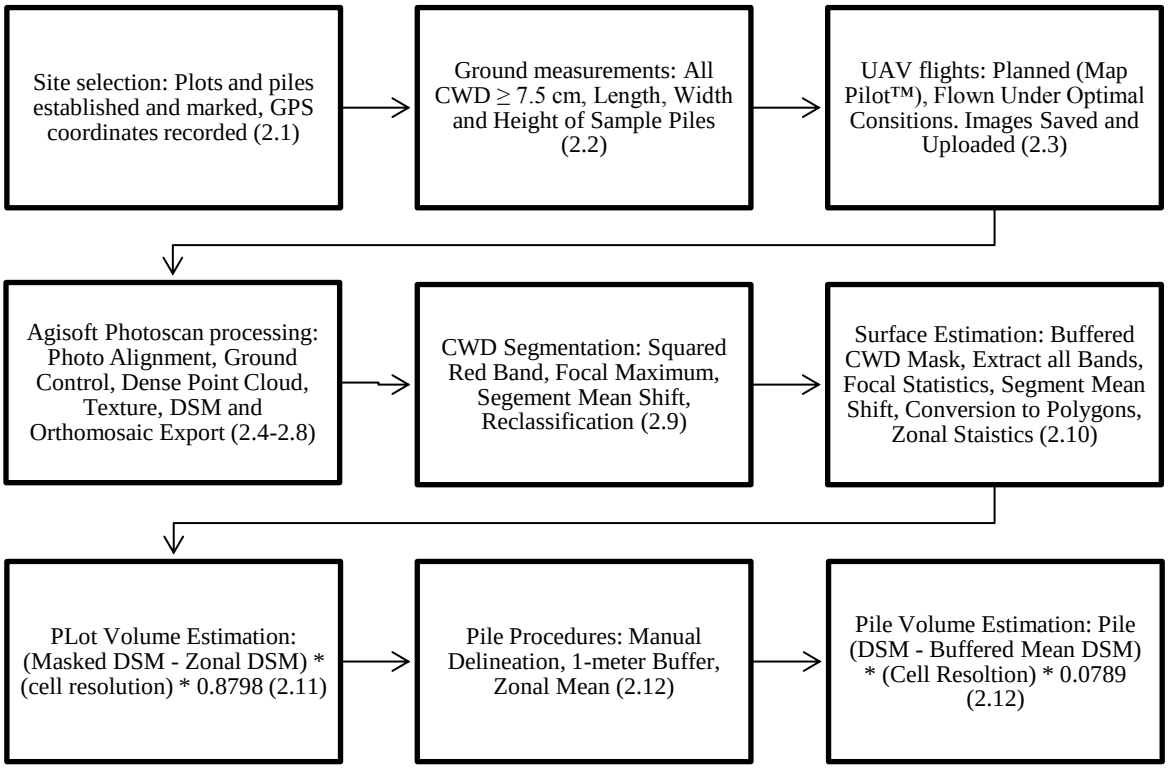

Figure 9: Generalized workflow for CWD volume estimation.

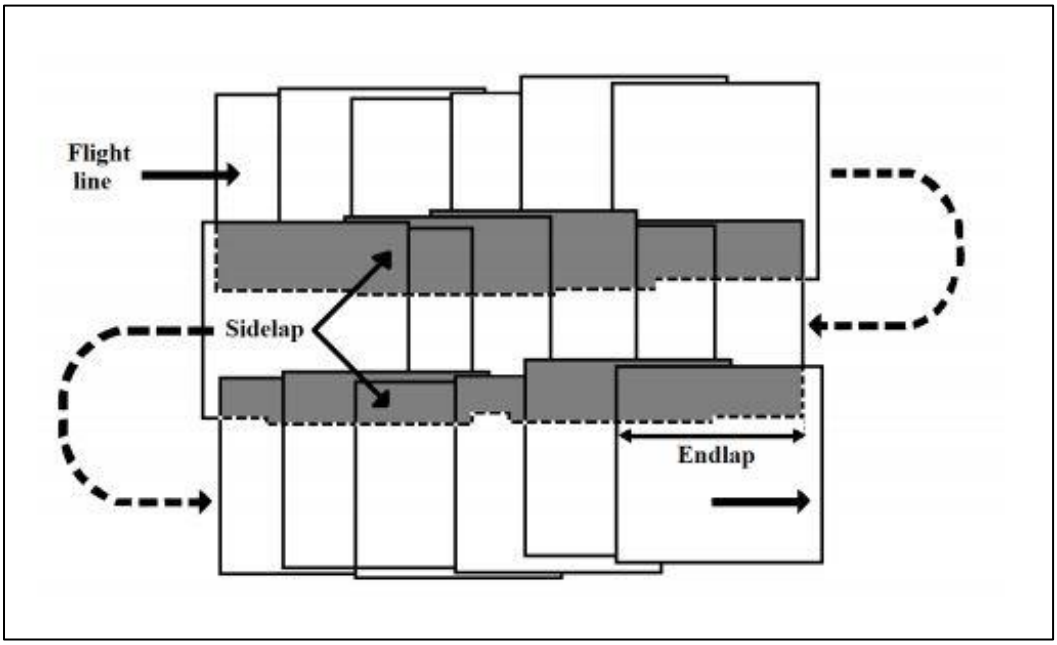

Figure 10: Sample flight plan for UAV.

2.4 Automatic Photo Alignment and Tie Point Generation

Common points on overlapping photos were located during the automatic photo alignment and tie point process. PhotoScan™ was instructed to use the highest accuracy setting, pair preselection was disabled, and the key point and tie point limits were set to zero.

2.5 Manual Location and Marking of Ground Control

Due to the high amount of overlap among photos, an individual ground control marker can be seen in multiple images. The GCPs were located and marked on each photo in which it appears. Assigning the real-world UTM coordinates and elevations to these markers unlocks the software's georeferenced export functionality.

2.6 Generation of Dense Point Cloud and Mesh Building

The dense point cloud is a collection of points attributed with the horizontal coordinates and vertical elevation. The elevations are computed using computer vision methods. The mesh is a polygonal surface created by connecting adjacent points in the point cloud. Both are required for the subsequent orthomosaic and terrain model generation processes. PhotoScan™ was instructed to build the point clouds with the highest quality and no depth filtering. The mesh was created from the dense point cloud using the arbitrary surface type, a zero-face count, and the extrapolated interpolation method enabled to ensure the entire surface is processed.

2.7 Building Texture

While not a requirement, the build texture process colorizes the point cloud to produce a photo-realistic representation of the site. This is useful for visualizing the site in three-dimensions. Texture was built using the generic mapping mode and a mosaic blending mode.

2.8 Building DSM and Orthomosaic and Exporting TIF

Before the surfaces are exported, internal DSM and orthomosaics must be generated. The DSM was built using the NAD 1983(HARN)/UTM 17N (EPSG: 3747) coordinate system and used the dense cloud as its source, interpolation enabled, and a pixel resolution less than 0.02 m/pix. The orthomosaic was generated using the same coordinate system based on the DSM surface, the mosaic blending mode, and a pixel resolution of 0.02 m/pix. The DSM and orthomosaics were then exported to the TIF format with cell sizes of 0.02 meters using the NAD 1983(HARN)/UTM 17N coordinate system.

2.9 CWD Segmentation

The first step in the approach in developing the bare ground surface is to locate and remove the coarse woody debris from the terrain surface. Visually, the red band, Band 3 of the orthomosaic provided the best discrimination between woody debris and bare ground (Figure 12). Areas containing woody debris have a higher spectral reflectance and therefore a higher pixel value than all other ground cover in this layer. Processing workflow for image enhancement on this layer was initiated by creating a new layer by squaring each pixel's value thus intensifying the bright CWD and minimizing the overall reflectance of other materials (Figure 13). Further intensification was carried out by running a 5x5 cell Focal Maximum filter across the squared image (Figure 14). This process expands the CWD zones slightly when it reassigns pixel values to match maximum value within a 5-cell window. Pixels in this new layer were then grouped based on similarities using the Segment Mean Shift tool (Figure 15). This tool groups pixels into segments based on both spectral and spatial similarities. Using an incremental approach, parameters for spectral detail, spatial detail, and minimum segment size parameters were set to a value of 18. Final CWD masks (Figure 16 and 17) were generated for each plot using either a thresholding technique where cutoff values were determined incrementally or an unsupervised classification. The unsupervised classification worked well at Jack's Creek. However, high reflectance and poor spectral differences at Rimes lead to the failure of the unsupervised classification. Thus, a thresholding technique was applied for Rimes. In this technique, cell values were incrementally classified. When the classification contained the best

Figure 11: Original Agisoft PhotoScan™ orthomosaic.

Figure 12: Orthomosaic red layer.

Figure 13: Squared orthomosaic red layer.

Figure 14: 5-cell by 5-cell Focal Maximum.

Figure 15: Mean segmented focal maximum.

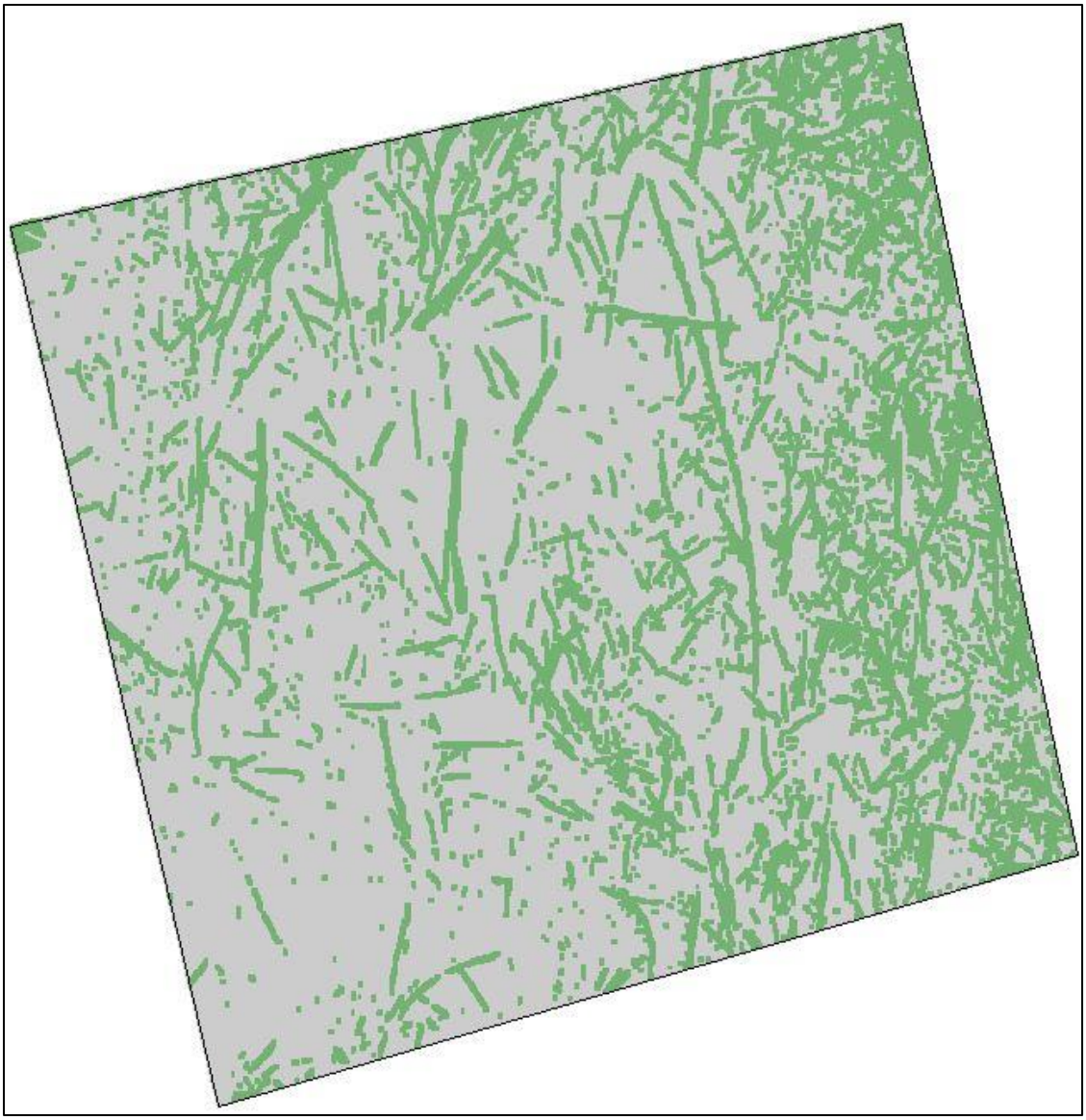

Figure 16: Reclassified segmented image.

Figure 17: Areas considered CWD.

representation of CWD, the classification was set for that plot. Each plot in a thresholding technique has unique values for the CWD class.

2.10 Estimating Surface Below CWD Mask

To estimate the surface below the CWD mask, a buffering approach was conducted. The CWD masked areas were expanded by 0.05 meters to contain the ground immediately adjacent to the CWD (Figure 18). That buffered image was relassified such that the CWD areas were assigned a value of one and everything else was assigned a value of zero. Each band of the orthophoto was extracted and Focal Statistics were generated (Figures 19 and 20). Two neighborhoods, 5x5 square cells and 9x9 square cells, and two Focal Statistics, mean and maximum, were used. The bands were then composited using the Composite Bands tool into a new image using only the areas within the buffered CWD mask (Figure 21). Using the Segment Mean Shift tool with all parameters set to 20, the new image was broken into zones with similar spectral charactaristics (Figure 22). Those segments were converted to polygons without allowing ESRI ArcMap™ to simplify the polygons. This allowed the zones to be used in a Zonal Statistics tool. Zonal means and minimums were calculated for each zone to create a digital surface model (DSM) (Figure 23).

2.11 Volume calculation

DSM values were extracted using the CWD mask. Volume is calculated by subtracting the masked DSM values from the mean or minimum DSM values created above and multiplying by cell size (0.02 m x 0.02 m) (*Equation 4*).

$$Vcell = (Masked\ DSM - Zonal\ [Mean]\ DSM) \cdot 0.02 \cdot 0.02 \quad (Equation\ 4)$$

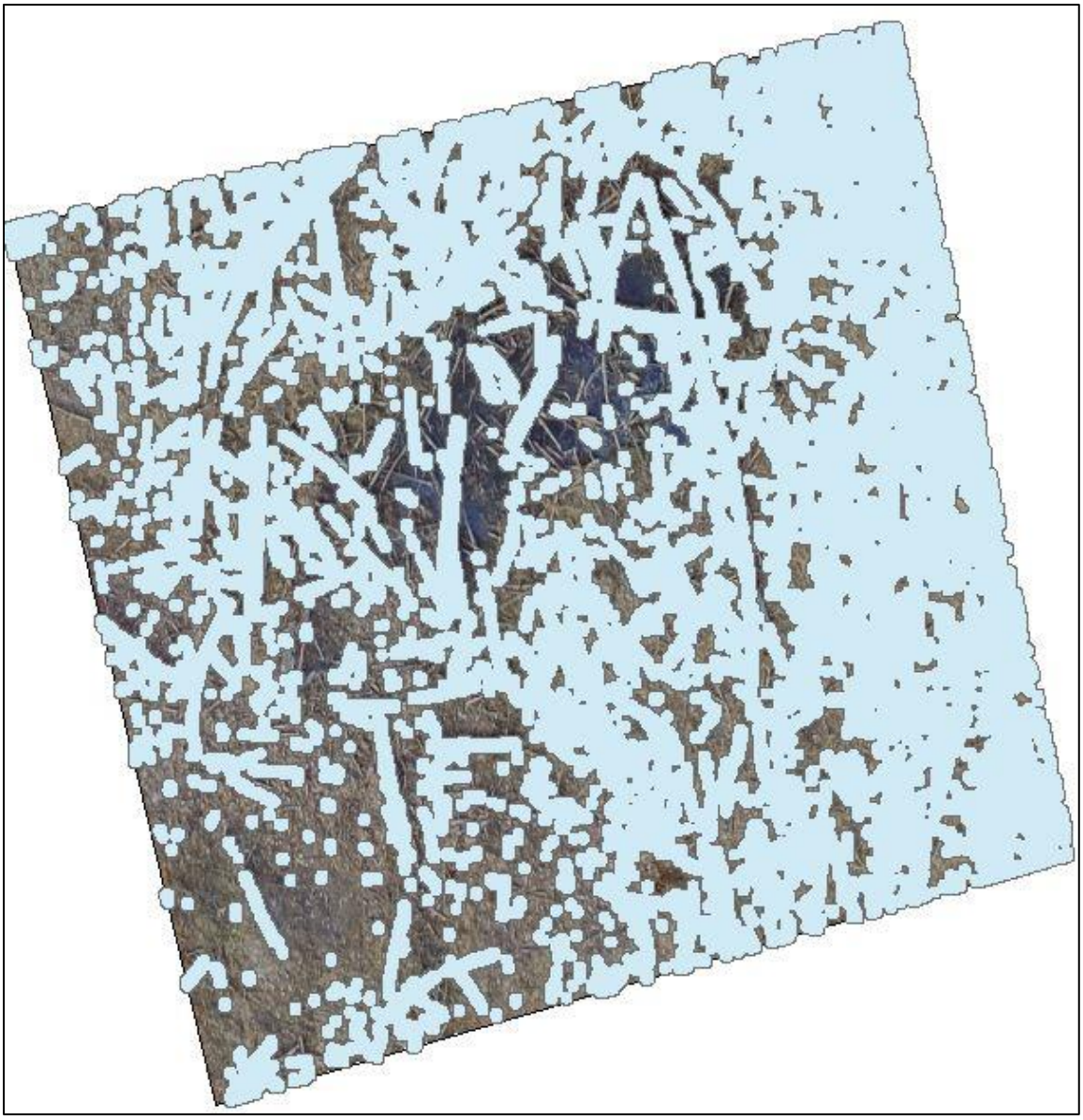

Figure 18: 0.05-m buffered CWD mask

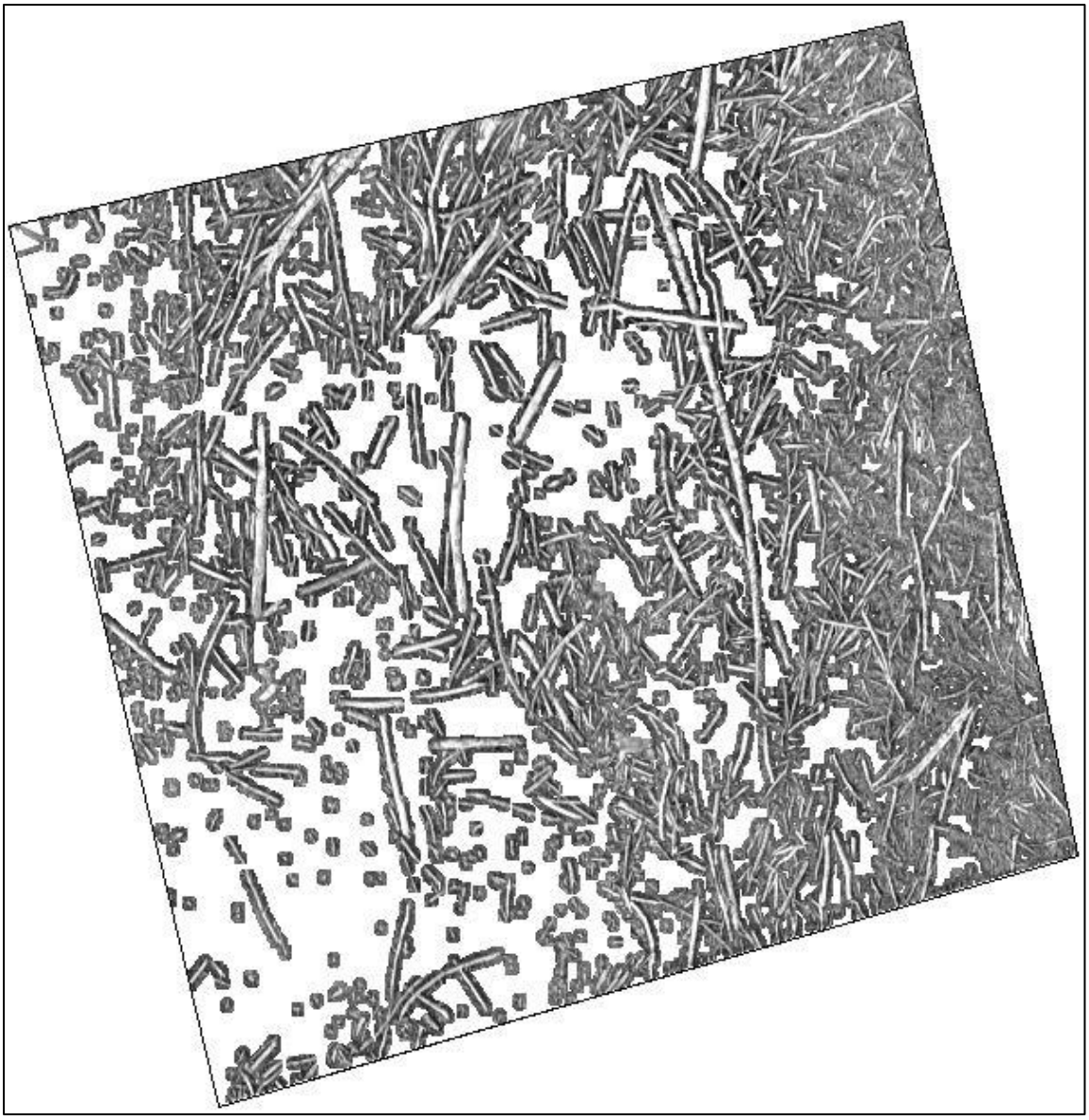

Figure 19: Extracted blue mask.

Figure 20: Focal mean blue mask.

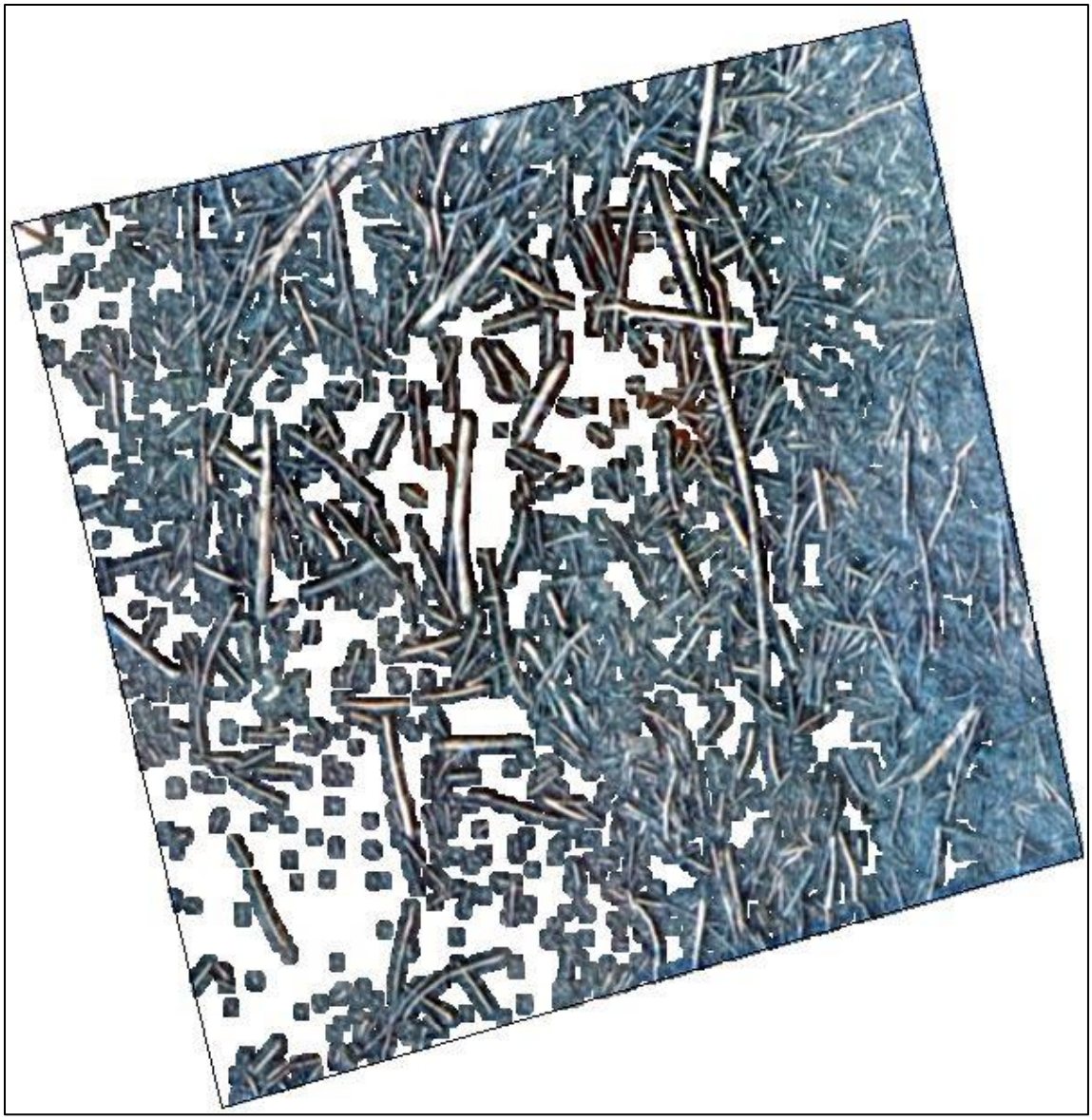

Figure 21: Composited focal mean masks.

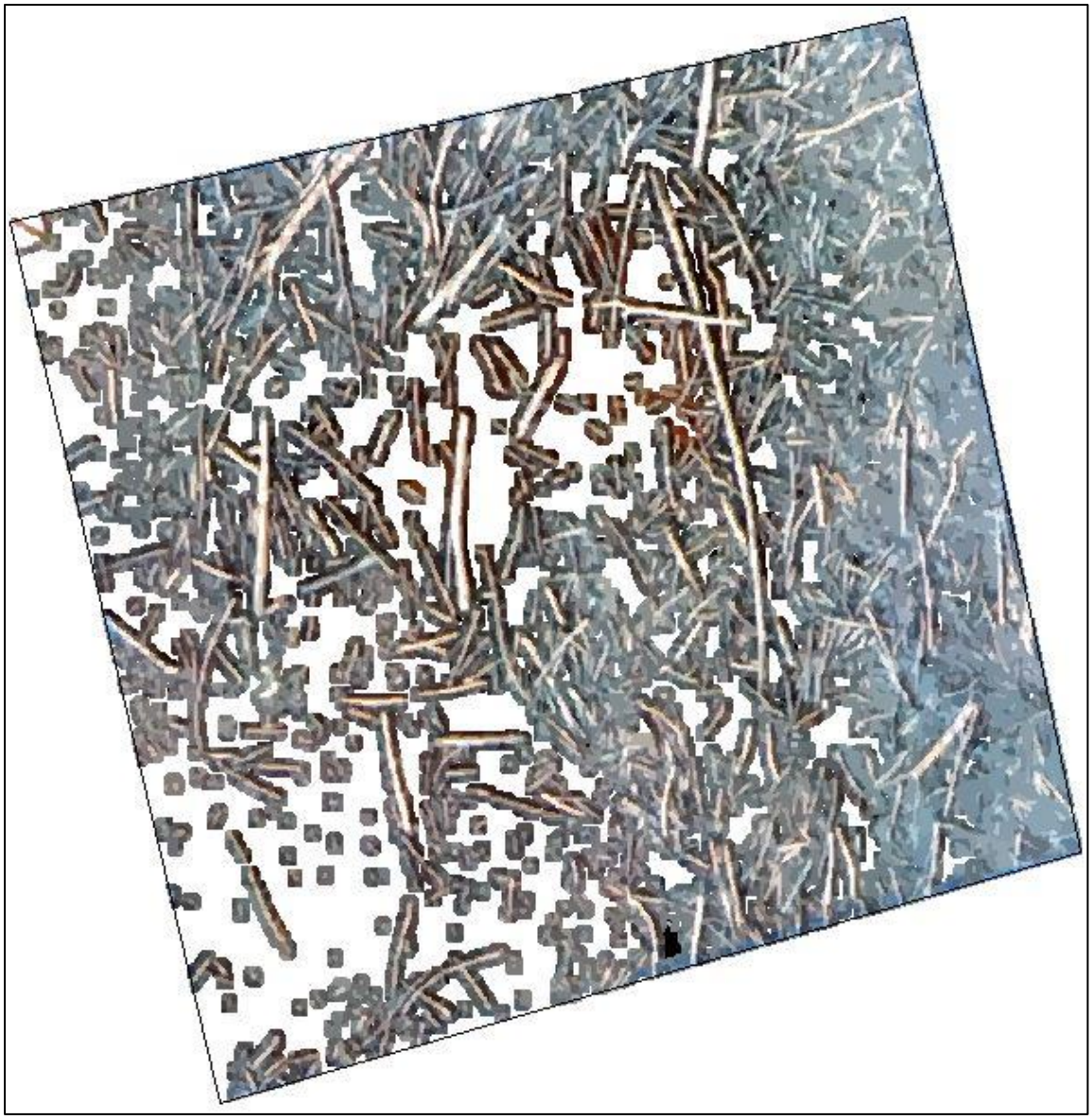

Figure 22: Mean segmented composite masks.

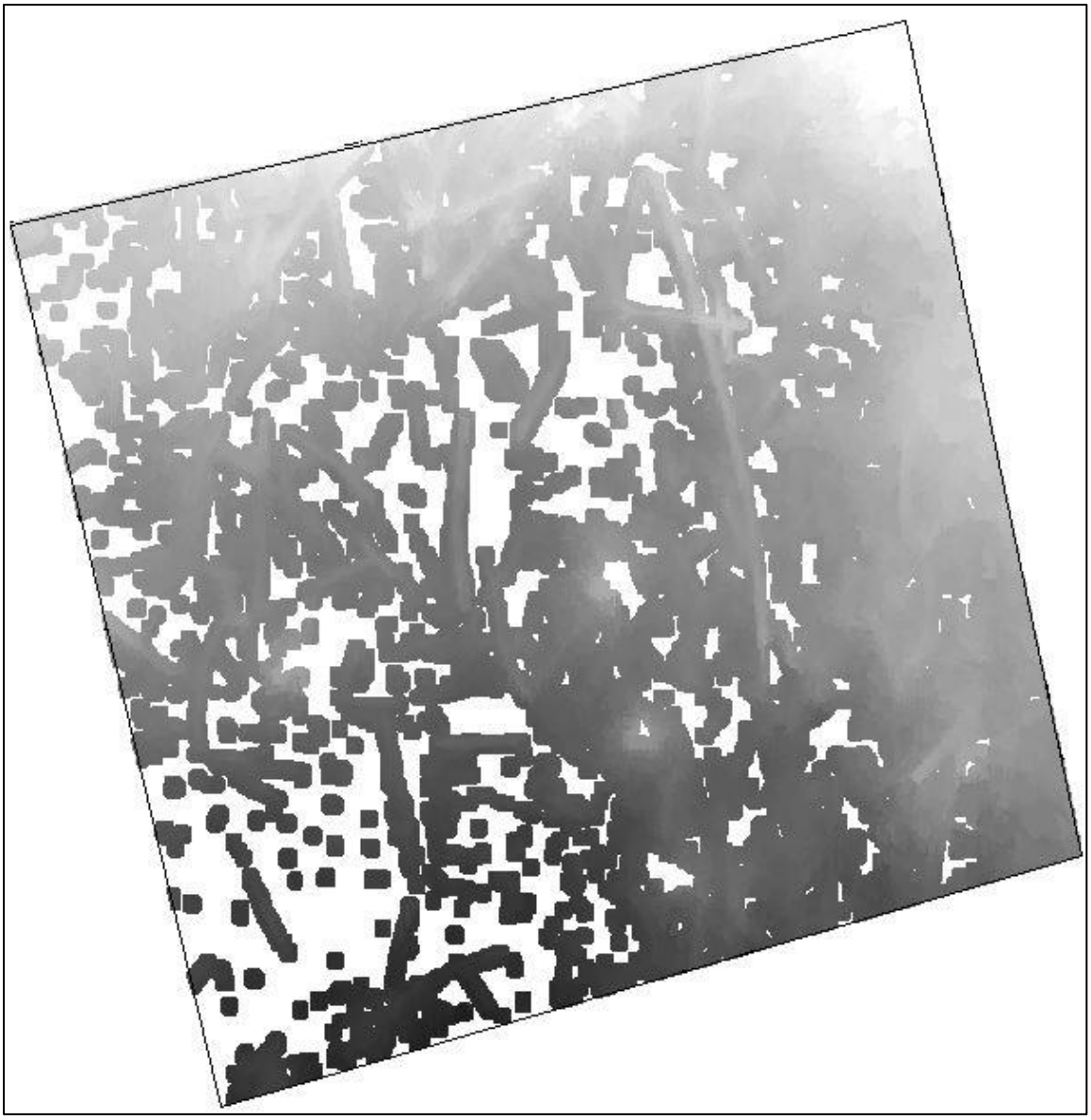

Figure 23: Zonal mean DSM.

All volume calculations were generated at the 0.02 m resolution and any cell yielding a negative volume was set to zero. These raw volume estimations do not consider the overestimation of volume by GIS for stems/CWD. The distributed slash volumes were multiplied by 0.8798 (from *Equation 2*) to account for stem overestimation.

2.12 Pile Procedures

Methods of estimating the volume of both oriented and slash piles differed from methods of estimating distributed woody debris in the 10-meter x 10-meter plots. First, each pile was manually delineated in ESRI ArcMap™. A 1-meter buffer around the pile was created. The mean elevation of the 1-meter buffer was used to estimate the ground elevation below the pile. The original DSM generated for the site was extracted for the delineated piles. *Equation 5* was used to calculate the uncorrected volume of each pile.

$$Vpile = (PileDSM - Buffer\ Mean\ DSM) \cdot 0.02 \cdot 0.02 (Equation\ 5)$$

The correction value of 0.0789 from Beauvais [25] was then applied to find the actual pile volume.

2.13 Comparison of UAV Estimated and Field Measured Volumes

To determine significance in differences between estimation methods, R 3.3.1 was used. T-Tests were conducted to determine what, if any, statistical significance exists between the UAV estimation method and the ground-based volume estimates.

CHAPTER 3

RESULTS

3.1 Jack's Creek Plots Using Mean Ground Measurement

For the nine measured 10 x 10 plots at the Jack's Creek site, the mean difference in ground-based volume estimation and drone-based volume estimation was 0.037 m^3 with a standard error of the mean of 0.105 m^3. The absolute value of individual plot estimate errors ranged from a low of 2% to a high of 281% (Appendix A). Using mean ground measurements, absolute value of errors ranged from 2% to 273% (Table 1). Comparing the sum of all ground measurements to the sum of all drone estimates resulted in -14% error. No significant difference was found between the ground-based and drone-based volume estimation ($p = 0.7362$, $df = 8$). A total site estimate of CWD volume, with 95% confidence interval, based on the ground measurements is 249 $m^3 \pm 148$ m^3. A total site estimate of CWD volume, with 95% confidence interval, based on the drone measurements is 290 $m^3 \pm 115$ m^3.

3.2 Rimes Plots Using Mean Ground Measurement

For the ten measured 10 m x 10 m plots at the Rimes site, the the mean difference in ground-based volume estimation and drone-based volume estimation was 0.038 m^3 with a standard error of the mean of 0.080 m^3. The absolute value of individual plot

Table 1:. Volume calculations for nine 10 x 10 m plots on Site Jack's Creek. Results are from mean DSM, 5 x 5 neighborhood, and focal mean. Ground values are the mean of multiple measurements.

Plot	Ground Volume	GIS Volume	Error
	----------m^3----------		--%--
jc_s01	0.161	0.143	-11
jc_s02	0.158	0.105	-34
jc_s03	0.989	0.197	-80
jc_s04	0.157	0.219	40
jc_s05	0.363	0.357	-2
jc_s06	0.149	0.554	273
jc_s07	0.051	0.138	170
jc_s08	0.097	0.134	38
jc_s09	0.204	0.151	-26
Overall	**2.329**	**1.998**	**-14**

estimate errors ranged from a low of 1% to a high of 842% (Appendix B). Using mean ground measurement values, the absolute value of errors ranged from 14% to 771% (Table 2). Comparing the sum of all ground measurements to the sum of all drone estimates resulted in -12% error. No significant difference was found between the ground-based and drone-based volume estimation ($p = 0.6467$, $df = 9$). A total site estimate of CWD volume, with 95% confidence interval, based on the ground measurements is 240 m^3 ± 79 m^3. A total site estimate of CWD volume, with 95% confidence interval, based on the drone measurements is 224 m^3 ± 73 m^3.

Table 2: Volume calculations for ten 10 x 10 m plots on Site Rimes. Results are from mean DSM, 5 x 5 neighborhood, and focal mean. Ground values are the mean of multiple measurements.

Plot	Ground Volume	GIS Volume	Error
	----------m^3----------		--%--
ri_s01	0.111	0.394	255
ri_s02	0.215	0.259	20
ri_s03	0.135	0.063	-53
ri_s04	0.487	0.245	-50
ri_s05	0.051	0.207	306
ri_s06	0.605	0.109	-82
ri_s07	0.394	0.089	-77
ri_s08	0.038	0.331	771
ri_s09	0.142	0.122	-14
ri_s10	0.123	0.209	-70
Overall	**2.301**	**2.028**	**-12**

3.3 All Plots at Both Sites

Using mean ground measurements for the 19 total plots at Jack's Creek and Rimes, the mean difference in ground-based volume estimation and drone-based volume estimation was 0.038 $m^3$with a standard error of the mean of 0.064 m^3. No significant difference was found between the ground-based and drone-based volume estimation ($p = 0.5627$, $df = 18$). Without using mean values for ground measurements (simply subtracting each ground measurement from the drone measurement), the mean difference in ground-based volume estimation and drone-based volume estimation was 0.023 m^3 with a standard error of the mean of 0.042 m^3. No significant difference was found between the ground-based and drone-based volume estimation ($p = 0.5857$, $df = 40$).

3.4 Difference Between Jack's Creek and Rimes

Since different approches were applied to Jack's Creek and Rimes in the CWD masking, the differences in ground and drone measurements for each site were compared. No significant difference was found between the two sites ($p = 0.992$, $df = 15$).

3.5 Jack's Creek Oriented Piles

For the seven measured oriented piles at the Jack's Creek site, the mean difference in ground-based volume estimation and drone-based volume estimation was 0.589 m^3 with a standard error of the mean of 0.232 m^3. Absolute values of individual pile estimate errors ranged from a low of 12% to a high of 53% with a mean error of 24% (Table 3). All but one pile was underestimated by the drone-based estimation. Comparing the sum of all ground measurements to the sum of all drone estimates resulted in -21% error. Significant difference was found between the ground-based and drone-based volume estimation ($p = 0.04457$, $df = 6$).

3.6 Rimes Slash Piles

For the nine measured slash piles at the Rimes site, the mean difference in ground-based volume estimation and drone-based volume estimation was 1.313 m^3 with a standard error of the mean of 0.447 m^3. Individual pile estimate errors ranged from a low of 11% to a high of 74% with a mean error of 43% (Table 4). All but one pile was underestimated by the drone-based estimation. Comparing the sum of all ground measurements to the sum of all drone estimates resulted in -44% error. Significant difference was found between the ground-based and drone-based volume estimation ($p = 0.0188$, $df = 8$).

Table 3: Volume calculations for seven oriented piles on Jack's Creek. Piles are manually delineated and the ground elevation is estimated using the mean value from a 1m buffer around the pile.

Plot	Ground Volume	GIS Volume	Error
	----------m^3----------		--%--
jc_p02	2.089	1.838	-12
jc_p03	3.571	2.646	-26
jc_p04	2.995	1.420	-53
jc_p05	2.058	2.446	19
jc_p06	3.330	2.463	-26
jc_p07	2.835	2.364	-17
jc_p08	2.361	1.938	-18
Overall	**19.239**	**15.115**	**-21**

Table 4: Volume calculations for seven oriented piles on Jack's Creek. Piles are manually delineated and the ground elevation is estimated using the mean value from a 1m buffer around the pile.

Plot	Ground Volume	GIS Volume	Error
	----------m^3----------		--%--
ri_p01	1.238	0.695	-44
ri_p02	1.963	1.579	-20
ri_p03	1.236	0.318	-74
ri_p04	1.452	0.672	-54
ri_p05	3.565	1.473	-59
ri_p06	4.426	2.349	-47
ri_p07	2.482	1.598	-36
ri_p08	8.998	4.693	-48
ri_p09	1.553	1.7163	11
Overall	**26.913**	**15.093**	**-44**

3.7 All Piles at Both Sites

For the 16 total piles at Jack's Creek and Rimes, the mean difference in ground-based volume estimation and drone-based volume estimation was 0.997 $m^3$with a standard error of the mean of 0.280 m^3. Significant difference was found between the ground-based and drone-based volume estimation ($p = 0.003814$, $df = 15$). The mean error for all piles was -35%.

3.8 Difference Between Oriented Piles and Slash Piles

Since Jack's Creek and Rimes had different types of piles, the differences in ground and drone measurements for each site were compared. No significant difference was found between the two sites ($p = 0.1769$, $df = 11.768$).

CHAPTER 4

DISCUSSION

4.1 10 m x 10m Plots

Drone estimates of the volume of woody residue, also known as coarse woody debris (CWD), ranged from very good (errors between 100% ground measurement and UAV were less than 10%) to poor (errors were greater than 70% when compared to ground measurements). The primary factor contributing to poor estimates was rough ground surface topography resulting from large-residual beds or rutting during harvest. However, areas with exposed sand that had high reflectance in the red band were also misclassified as woody residue. Rainfall also plays a role on these poorly drained sites. Heavy rainfall during our measurements impacted the Jack's Creek site. Some plots were flooded during the second measurement and during the flights (Figure 24). It is possible that CWD was relocated while the plot was flooded. Moreover, for flooded plots, the UAV would not be able to gather imagery for any CWD under water. However, the rains could have benefitted in increasing contrast between the CWD and the soil. The rains did not seem impact the Rimes site negatively.

Figure 24: Plot jc_s2 after heavy rains on 1/5/2017. Heavy rains flooded some plots at the Jack's Creek site.

The topography of the plots and soil spectral characteristics played a factor in CWD segmentation. Areas of rough topography from bedding during planting or rutting during harvest resulted in higher errors for volume estimation (Figure 25). The Jack's Creek site contained a perennial stream. Thus, many plots showed heavy rutting from harvest activity. Rutting was not as severe at the Rimes site. However, bedding still caused some problems in volume estimation at the Rimes site. Moreover, the high reflectance of sand in area resulted in poor CWD segmentation (Figures 26 and 27). The bedding in this site exposed large areas of sand. In plots with a large area of exposed sand, CWD segmentation failed. It is possible that improved cameras with NIR would help to resolve this issue. However, this study did not have access to such a camera.

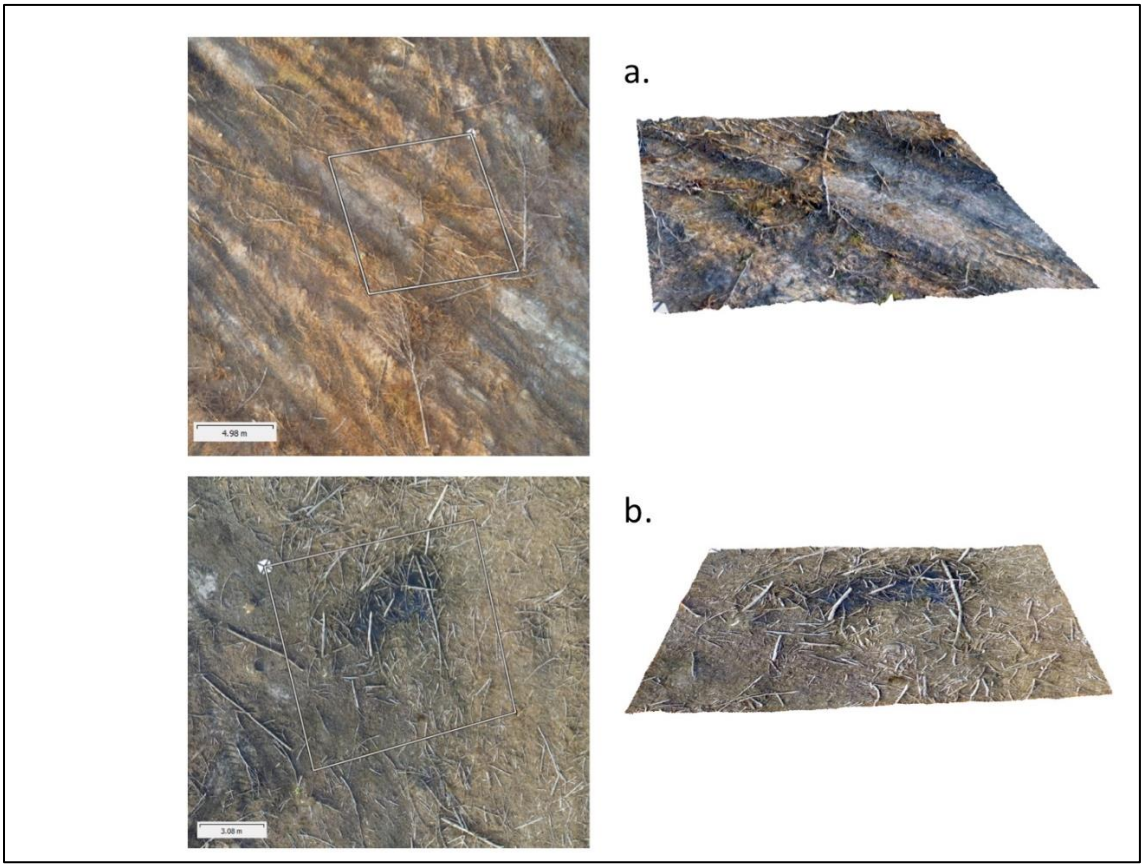

Figure 25: Example of a 10 x 10 m plot where drone-based estimates of woody residue volume had a high error due to the large amount of ground surface microtopography (a) and a plot where drone estimates of woody residue volume differed from ground measurements by less than 10% (b). Aerial image and 3-dimensional reconstruction are shown for both plots.

Figure 26: Example CWD segmentation for plot jc_s01 at Jack's Creek in which the segmentation process worked well.

Figure 27: Example CWD segmentation for plot jc_s07 at Jack's Creek in which the segmentation process failed due to the high reflectance of sand.

4.2 Jack's Creek Oriented Piles

Drone estimates of oriented pile volume ranged from good (errors were less than 30% when compare to ground measurement) to poor (errors less than 70% when compared to ground measurements). One oriented pile fell into the poor category with the other six either in the good category. In fact, four piles had errors less than 20%. It is possible that the mean value from the buffered area did not accurately represent the ground elevation around the piles. Some piles were close together and the 1-meter buffer could have incorporated some large stems from another pile (Figure 28).

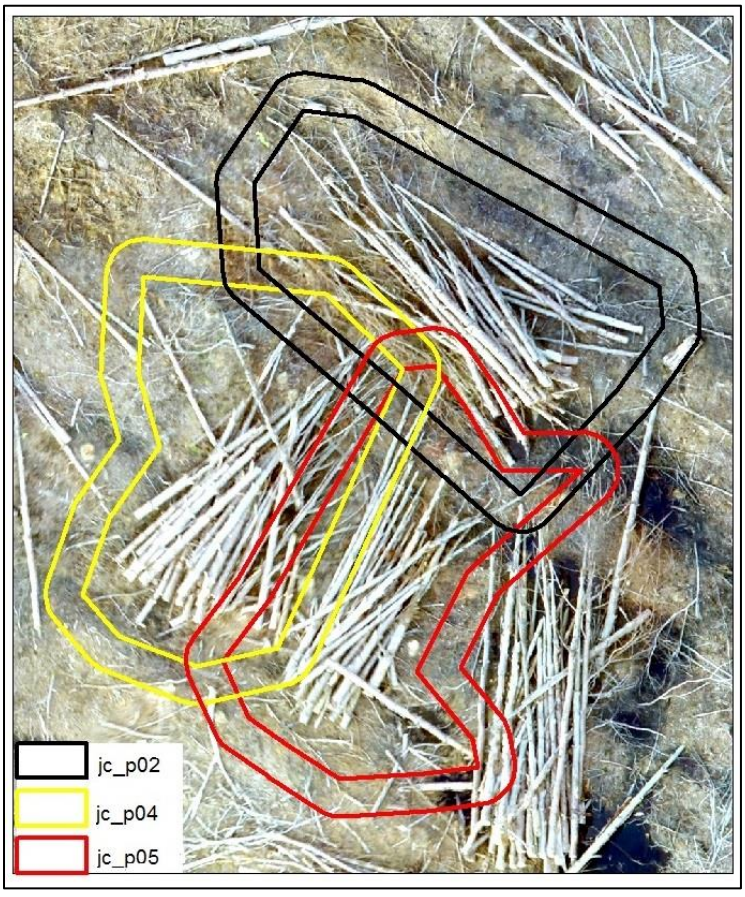

Figure 28: Jack's Creek piles (jc_p02, jc_p04, jc_p05) and their corresponding 1m buffer. Some buffers ran over into neighboring piles possibly impacting ground elevation estimation.

4.3 Rimes Slash Piles

Drone estimates of slash pile volume ranged from good (errors were less than 30% when compare to EEP ground measurement) to poor (errors were greater than 70% when compared to EEP ground measurements). However, only one pile fell into the poor category. All but one pile were underestimated by the UAV method. The under estimation of the slash piles could also be a result of the mean value from the buffered area not accurately representing the ground elevation around the piles. However, as the slash piles at the Rimes site were more evenly distributed across the site, the mean value from the buffered area is likely an accurate representation of the ground elevation at the piles (Figure 29). Another possible source of error is the fine resolution of the imagery. At 2-cm resolution, the GIS software is capturing much more surface roughness than the ground-based measurements are. Moreover, the half-ellipsoid equation was used for each pile. Some piles might have been more accurately described as another form. This could result in some error in volume estimation on the ground side. However, based on visual observations, the half-ellipsoid equation appeared the most appropriate for nearly all, if not all, the piles measured.

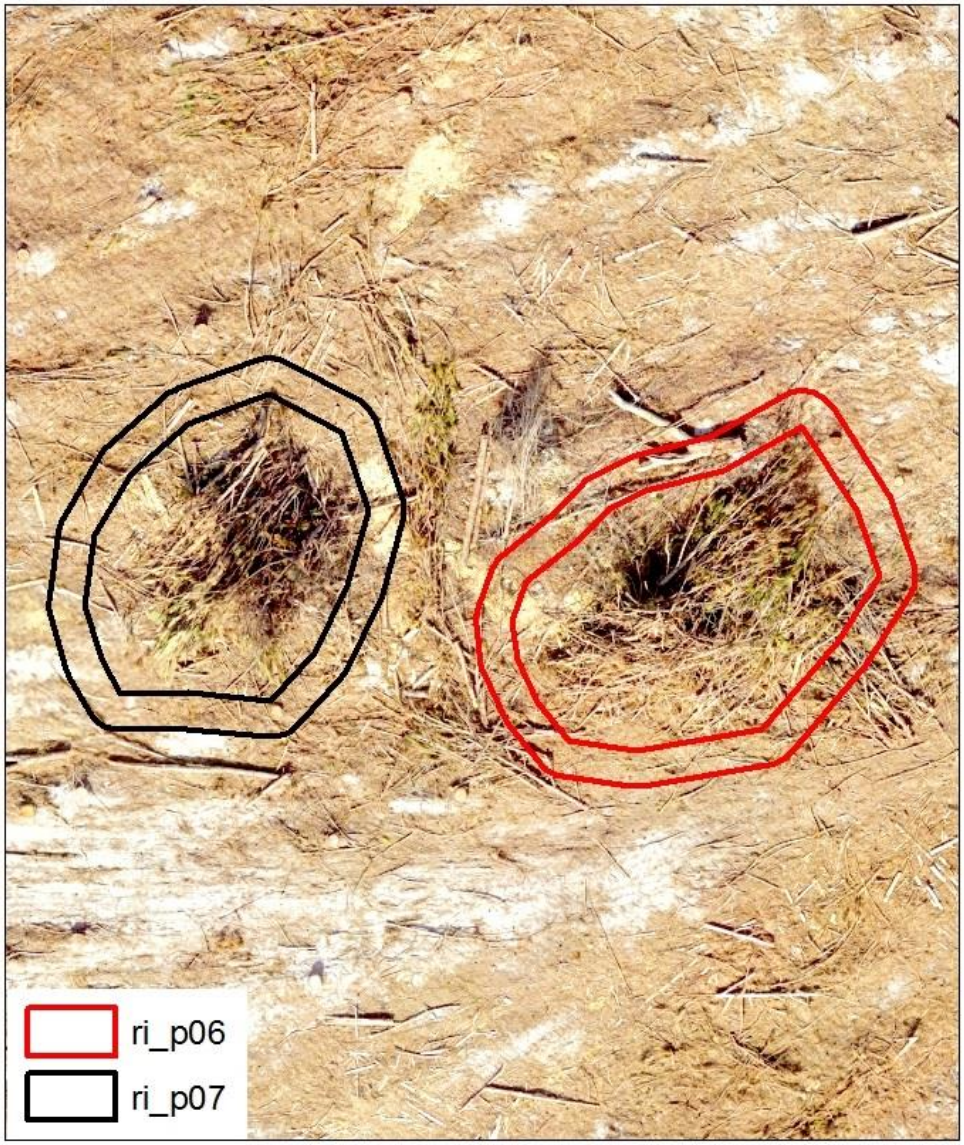

Figure 29: Piles from the Rimes sites (ri_p06 and ri_p07) and their corresponding buffers. No buffers overlapped other piles in the Rimes site.

4.4 All Piles Across Both Sites

The mean error of all piles across both sites was 35.06%. Using the study of Trofymow et al. [14] as a benchmark, the estimates were over the expected error of 20%. Again, the error could lie in the application of EEP, which was shown to produce the highest estimates of pile volume [14]. Slash piles produced a greater underestimation than did oriented piles. This is likely due to the denser nature of the oriented piles. There is more wood volume in a smaller total area in the oriented piles as compared to the slash piles.

4.5 Future Research

Overall, our results suggest that further research using an upgraded camera with NIR or red edge capabilities is warranted. The upgraded camera would allow users to quickly distinguish between living and cut plants. It is possible that NIR or red edge would also help to distinguish between the ground and CWD. Wetter objects have greater reflectance in the NIR spectrum. Thus, soils, especially wet soils, could show high contrast when compared to CWD. Moreover, more analysis of the ratio of drone-based volumes to ground-based volumes is needed. An approach that combines the ground-based volume measurements of Beauvais [25] with the drone-based volume estimates in this study could establish an appropriate ratio for future use. Finally, other approaches could be used to classify the CWD on a plot. The use of computer vision (CV) offers promise in automating CWD classification. CV has been used to analyze a variety of objects such as produce, wine, and salmon [31-33]. CV has been used to date tree rings as well [34]. Moreover, researchers from the University of Georgia's Center for Geospatial Research were able to use CV to isolate downed trees after a storm in the

Smokey Mountains [35]. If these methods can be adopted to CWD detection and classification, it could result in a better classification that eliminates some of the errors associated with the reflectance of sand or other substrates. CV, combined with an upgraded camera and better pile ratios, could return estimates that are improved from this study.

A non-fixed variance model was created to attempt to predict ground measurements from the air (UAV) measurements with a 95% confidence interval (Figure 30). This model is only preliminary and can be refined using the SIMEX method. However, this model, once properly calibrated with enough data points, can serve as a tool for users to accurately estimate ground (true) volume with UAV estimates without the need for continual ground truthing. Only periodic calibration to increase accuracy of the model would be needed.

Finally, a simpler approach to calculating the volume of the scattered slash in the 10-meter x 10-meter plots will be conducted. Using the CWD masked created in this project, an attempt will be made to measure the length and diameter of each piece on CWD identified. These measurements will allow for a volume calculation independent of the ground surface elevation and could reduce uncertainties associated with rough topography from bedding or rutting.

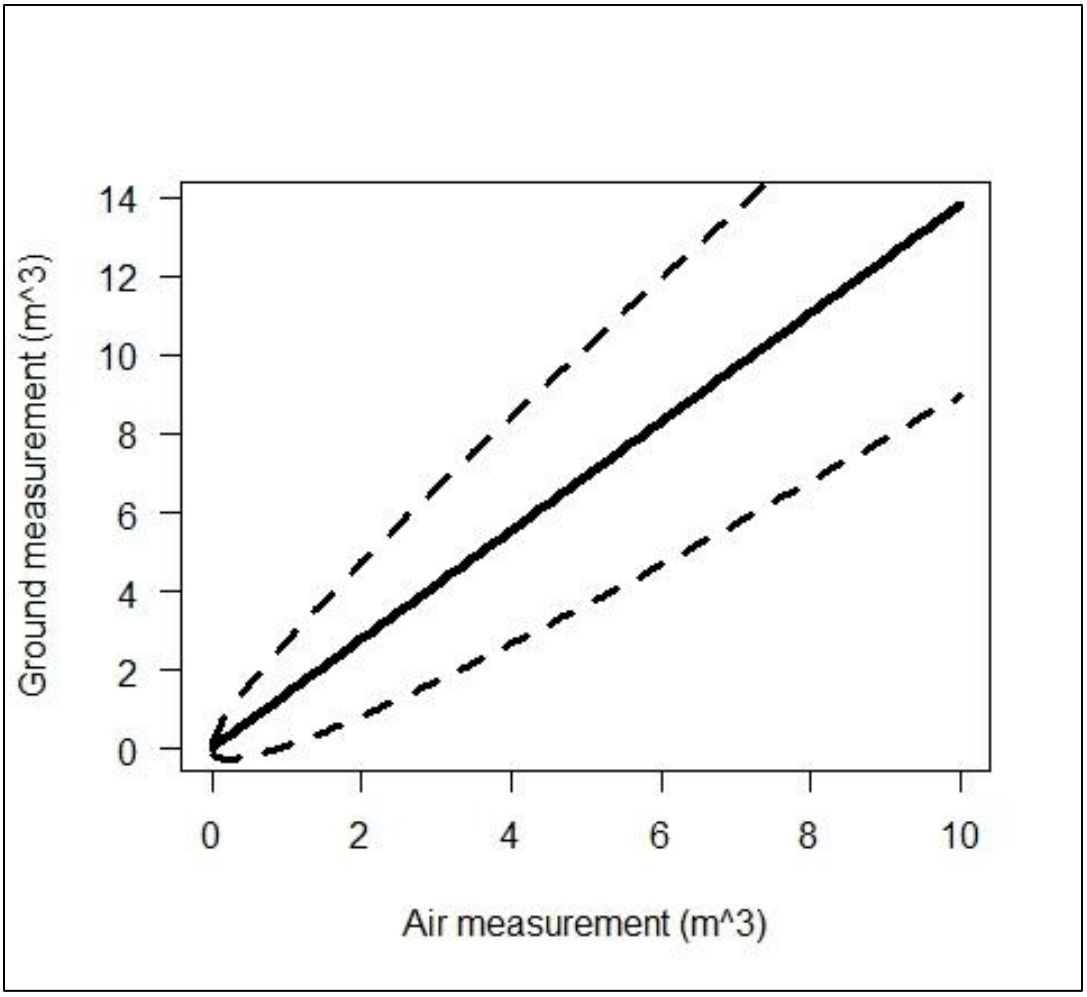

Figure 30: Non-fixed variance model to predict ground measurements from air (UAV) measurements.

CHAPTER 5

CONCLUSIONS

A typical harvest site will include areas of very rough ground surface as well as areas of flatter ground. We captured both extremes as well as more typical areas in our analyses. If very rough areas of ground surface are avoided in sampling, and we assume that residue distribution is not correlated with ground surface roughness, drone-based estimates of residues are as accurate or more accurate as ground measurements estimates using line intercept sampling. This process is quicker and more cost effective than traditional sampling methods.

Pile volumes were consistently underestimated when compared to ground estimates. Oriented piles are generally estimated more accurately than slash piles with mean errors of 24.28% and 43.44% respectively. Given the methods of ground-based volume estimation, the oriented pile volumes are most likely more accurate. Thus, it would be reasonable to conclude the drone-based approach underestimates pile volumes by around 25%. The errors for estimates of slash piles fall in line with previous studies [14].

Despite with the errors and uncertainties found in this study, it produced estimates that are useful for users. With calibration and correction, it has the potential to save time and money for companies wishing to use CWD for energy production. The UAV

methods decrease operational costs while increasing productivity. While traditional field sampling could take a week or longer to complete with several people doing the field sampling, a site could be sampled and processed within a few days of harvest with as little as an hour devoted to field sampling.

REFERENCES

1. Shaw, C.H., et al., *The relationships of soil fauna to long-term forest productivity in temperate and boreal ecosystems: processes and research strategies.* FRI Bulletin, 1991(161): p. 39-77.
2. Weston, C.J. and K.L. Whittaker, *Soils and site: soil biology.* Encyclopedia of Forest Sciences, 2004.
3. Morris, L.A., *Soil Organic Matter Forms and Functions.* Encyclopedia of Forest Sciences, 2004: p. p. 1202-1207.
4. Page-Dumroese, D., et al., *Soil quality is fundamental to ensuring healthy forests [electronic resource]*, in *Advances in threat assessment and their application to forest and rangeland management / [edited by] John M. Pye ... [et al.]*. 2010, Portland, OR : U.S. Dept. of Agriculture, Forest Service, Pacific Northwest Research Station, 2010. General technical report PNW ; GTR-802. p. 27-36.
5. Milbrandt, A., *Geographic Perspective on the Current Biomass Resource Availability in the United States*. 2005.
6. REN21, *Renewables 2013 Global Status Report*, in *Renewables 2013 Global Status Report*. 2013, (Paris: REN21 Secretariat).
7. IRENA, *Global Bioenergy: Supply and Demand Projections, a working paper for Remap 2030*, in *International Renewable Energy Agency (IRENA)*. 2014, International Renewable Energy Agency (IRENA): Abu Dhabi, United Arab Emirates.
8. Wagner, C.E.v., *The line intersect method in forest fuel sampling.* Forest Science, 1968. **14**(1): p. 20-6.

9. Woldendorp, G., et al., *Analysis of sampling methods for coarse woody debris.* Forest ecology and management, 2004. **198**(1-3): p. 133-148.

10. Long, J.J. and K. Boston, *An Evaluation of Alternative Measurement Techniques for Estimating the Volume of Logging Residues.* Forest Science, 2014. **60**(1): p. 200-204.

11. Macfadyen, A. and E.D. Ford, *Advances in ecological research. Volume 16*. 1987: Academic Press Inc.,Orlando, FL.

12. Nemec, A.F.L. and G. Davis, *Efficiency of Six Line Intersect Sampling Designs for Estimating Volume and Density of Coarse Woody Debris*. 2002, Research Section, Vancouver Forest Region, BC Ministry of Forests, Nanaimo. p. 12.

13. Pickford, S.G. and J.W. Hazard, *Simulation Studies on Line Intersect Sampling of Forest Residue.* Forest Science, 1978. **24**(4): p. 469-483.

14. Trofymow, J.A., N.C. Coops, and D. Hayhurst, *Comparison of remote sensing and ground-based methods for determining residue burn pile wood volumes and biomass.* Canadian Journal of Forest Research-Revue Canadienne De Recherche Forestiere, 2014. **44**(3): p. 182-194.

15. Popescu, S.C., R.H. Wynne, and R.F. Nelson, *Measuring individual tree crown diameter with lidar and assessing its influence on estimating forest volume and biomass.* Canadian Journal of Remote Sensing, 2003. **29**(5): p. 564-577.

16. Eamer, J.B.R. and I.J. Walker, *Quantifying sand storage capacity of large woody debris on beaches using LiDAR.* Geomorphology, 2010. **118**(1–2): p. 33-47.

17. Tseng, C.M., et al., *Application of a multi-temporal, LiDAR-derived, digital terrain model in a landslide-volume estimation.* Earth Surface Processes and Landforms, 2013. **38**(13): p. 1587-1601.

18. Hummel, S., et al., *A Comparison of Accuracy and Cost of LiDAR versus Stand Exam Data for Landscape Management on the Malheur National Forest.* 2011. **109**(5): p. 267-273.

19. Tomlinson, R.F., *A geographic information system for regional planning*. 1968, Macmillan Company of Australia : South Melbourne, Victoria, Australia: Australia. p. 200-210.

20. James, M.R. and S. Robson, *Mitigating systematic error in topographic models derived from UAV and ground-based image networks.* Earth Surface Processes and Landforms, 2014. **39**(10): p. 1413-1420.

21. Satterwhite, M.B. and J.P. Henley, *Spectral Characteristics of Selected Soils and Vegetation in Northern Nevada and Their Discrimination Using Band Ratio Techniques.* Remote Sensing of Environment, 1987. **23**(2): p. 155-175.

22. Tang, Q., et al., *Assessment of soil erosion using RUSLE and GIS: a case study of the Yangou watershed in the Loess Plateau, China.* Environmental Earth Sciences, 2015. **73**(4): p. 1715-1724.

23. Teixeira, J., et al., *A comprehensive analysis of groundwater resources using GIS and multicriteria tools (Caldas da Cavaca, Central Portugal): environmental issues.* Environmental Earth Sciences, 2014. **73**(6): p. 2699-2715.

24. Castedo, R., et al., *Measurement of historical cliff-top changes and estimation of future trends using GIS data between Bridlington and Hornsea - Holderness Coast (UK).* Geomorphology, 2015. **230**: p. 146-160.

25. Westoby, M.J., et al., *'Structure-from-Motion' photogrammetry: A low-cost, effective tool for geoscience applications.* Geomorphology, 2012. **179**: p. 300-314.

26. Shields, J.A., et al., *Spectrophotometric measurement of soil color and its relationship to moisture and organic matter.* Canadian Journal of Soil Science, 1968. **48**(3): p. 271-280.

27. *Brush disposal forest practice guidebook.* 2005 [cited 2016 27 September].

28. Beauvais, C., *Coarse woody debris in a loblolly pine plantation managed for biofuel production*. 2010, Duke University.

29. Hardy, C.C., *Guidelines for estimating volume, biomass, and smoke production for piled slash. Forest Service general technical report*. 1996.

30. Grenzdorffer, G.J., A. Engel, and B. Teichert, *The Photogrammetric Potential of Low-Cost UAVS in Forestry and Agriculture.* INTERNATIONAL ARCHIVES OF PHOTOGRAMMETRY REMOTE SENSING AND SPATIAL INFORMATION SCIENCES, 2008. **37**(3): p. 1207-1214.

31. Cardenas-Perez, S., et al., *Evaluation of the ripening stages of apple (Golden Delicious) by means of computer vision system.* Biosystems Engineering, 2017. **159**: p. 46-58.

32. Conde, B.C., et al., *Development of a robotic and computer vision method to assess foam quality in sparkling wines.* Food Control, 2017. **71**: p. 383-392.

33. Jun-Li, X., C. Riccioli, and S. Da-Wen, *Comparison of hyperspectral imaging and computer vision for automatic differentiation of organically and conventionally farmed salmon.* Journal of Food Engineering, 2017. **196**: p. 170-182.

34. Subah, S., S. Derminder, and C. Sanjeev, *An interactive computer vision system for tree ring analysis.* Current Science (00113891), 2017. **112**(6): p. 1262-1265.

35. Bernardes, S. and M. Madden, *Vegetation disturbance and recovery following a rare windthrow event in the Great Smoky Mountains National Park.* Archives of the International Society for Photogrammetry and Remote Sensing (submitted), 2016.

APPENDIX A

JACK'S CREEK PLOT COMPARISONS

Plot	Ground Volume	GIS Volume	Error
	----------m^3----------		--%--
jc_s01	0.140	0.143	2
jc_s01	0.182	0.143	-22
jc_s02	0.145	0.105	-28
jc_s02	0.170	0.105	-38
jc_s03	0.954	0.197	-79
jc_s03	1.024	0.197	-81
jc_s04	0.151	0.219	46
jc_s04	0.163	0.219	35
jc_s05	0.340	0.357	5
jc_s05	0.386	0.357	-7
jc_s06	0.152	0.554	281
jc_s06	0.146	0.554	265
jc_s07	0.057	0.138	205
jc_s07	0.045	0.138	142
jc_s08	0.111	0.134	60
jc_s08	0.084	0.134	21
jc_s09	0.193	0.151	-22
jc_s09	0.215	0.151	-30

APPENDIX B

RIMES PLOT COMPARISONS

Plot	Ground Volume	GIS Volume	Error
	----------m^3----------		--%--
ri_s01	0.112	0.394	252
ri_s01	0.110	0.394	258
ri_s02	0.239	0.259	8
ri_s02	0.209	0.259	24
ri_s02	0.198	0.259	31
ri_s03	0.128	0.063	-51
ri_s03	0.138	0.063	-54
ri_s03	0.138	0.063	-54
ri_s04	0.487	0.245	-50
ri_s04	0.487	0.245	-50
ri_s05	0.054	0.207	286
ri_s05	0.049	0.207	320
ri_s06	0.592	0.109	-82
ri_s06	0.618	0.109	-82
ri_s07	0.352	0.089	-75
ri_s07	0.436	0.089	-80
ri_s08	0.043	0.331	662
ri_s08	0.036	0.331	811
ri_s08	0.035	0.331	842
ri_s09	0.120	0.122	1
ri_s09	0.163	0.122	-26
ri_s10	0.128	0.208	62
ri_s10	0.117	0.208	77